GFZ
Helmholtz-Zentrum
POTSDAM

HELMHOLTZ-ZENTRUM POTSDAM
DEUTSCHES
GEOFORSCHUNGSZENTRUM

Owolabi, C., Ruan, H., Yamazaki, Y., Kaka, R. O., Akinola, O. O., Yoshikawa, A. (2022): Ionospheric Current Variations by Empirical Orthogonal Function Analysis: Solar Activity Dependence and Longitudinal Differences. - Journal of Geophysical Research: Space Physics, 127, 1, e2021JA029903.

https://doi.org/10.1029/2021JA029903

Institional Repository GFZpublic: https://gfzpublic.gfz-potsdam.de/

Check for updates

JGR Space Physics

RESEARCH ARTICLE
10.1029/2021JA029903

Key Points:

- Empirical model of the Sq current has been constructed based on geomagnetic data obtained over the American and European/African sectors
- Sq current functions are decomposed into dominant eigenmodes with 96% of the total variance being captured, leading to a robust empirical orthogonal function model
- Sq current intensity is significant at equinoxes in both sectors, with asymmetry between the northern and southern hemispheres

Correspondence to:
H. Ruan,
rhb@nuist.edu.cn

Citation:
Owolabi, C., Ruan, H., Yamazaki, Y., Kaka, R. O., Akinola, O. O., & Yoshikawa, A. (2022). Ionospheric current variations by empirical orthogonal function analysis: Solar activity dependence and longitudinal differences. *Journal of Geophysical Research: Space Physics*, *127*, e2021JA029903. https://doi.org/10.1029/2021JA029903

Received 21 AUG 2021
Accepted 5 DEC 2021

Author Contributions:
Conceptualization: Charles Owolabi
Data curation: Akimasa Yoshikawa
Funding acquisition: Haibing Ruan
Investigation: Charles Owolabi
Methodology: Charles Owolabi
Supervision: Haibing Ruan, Y. Yamazaki
Validation: Haibing Ruan, Y. Yamazaki, O. O. Akinola
Visualization: R. O. Kaka, O. O. Akinola
Writing – original draft: Charles Owolabi
Writing – review & editing: Charles Owolabi

© 2021. American Geophysical Union. All Rights Reserved.

Ionospheric Current Variations by Empirical Orthogonal Function Analysis: Solar Activity Dependence and Longitudinal Differences

Charles Owolabi[1,2], Haibing Ruan[3], Y. Yamazaki[4], R. O. Kaka[5], O. O. Akinola[6], and Akimasa Yoshikawa[7]

[1]Department of Earth and Space Sciences, Southern University of Science and Technology, Shenzhen, China, [2]Department of Physics, Federal University of Technology Akure, Akure, Nigeria, [3]School of Remote Sensing and Geomatics Engineering, Nanjing University of Information Science and Technology, Nanjing, China, [4]GFZ German Research Centre for Geosciences, Potsdam, Germany, [5]Bradley Department of Electrical and Computer Engineering, Virginia Polytechnic Institute and State University, Blacksburg, VA, USA, [6]Centre for Atmospheric Research, National Space Research and Development Agency, Abuja, Nigeria, [7]International Center for Space Weather Science and Education, Kyushu University, Fukuoka, Japan

Abstract The solar quiet (Sq) ionospheric current variations exhibit spatial and temporal patterns that can be identified by the prevailing eigenmodes based on the empirical orthogonal function (EOF) analysis. In this study, the Sq current function over the American and European/African sectors are derived using ground magnetometer data from 2006 to 2019 based on the spherical harmonic analysis technique. Subsequently, we decomposed the Sq current function into eigenmodes by applying the EOF analysis, where the first three eigenmodes capture 96% of the overall Sq current variance. Additionally, these eigenmodes are utilized to model the Sq current function and compare its properties between the two longitudinal sectors. We observed that the EOF model could reconstruct the observed Sq current function with the first three eigenmodes in both longitudinal sectors. Moreover, the EOF model unveils a clear association of the Sq current function with several driven features, such as magnetic latitude, local time, season, and solar activity. Both longitudinal sectors had comparable Sq current patterns under varying solar activity, while their amplitudes varied. Besides, the newly developed model could reproduce a refined Sq current variability over the two longitudinal sectors as long as the observed Sq variations have sufficient duration. Our EOF model shows that the variations of the Sq current function with solar activity can be explained by the first three eigenmodes, which could be used as a basis for further numerical modeling of the Sq current variations.

Plain Language Summary Electromagnetic fields and currents in the E-region ionosphere induce solar quiet (Sq) geomagnetic variations responsible for Sq current variation. In order to fully explain the Sq current characteristics, including its spatial and temporal variability, it is necessary to continue to garner an understanding of its complexities. On the basis of the spherical harmonic analysis of the geomagnetic Sq variations, we computed the Sq current function over the American and European/African sectors. We next utilized empirical orthogonal function (EOF) analysis to decompose the Sq current function into dominant spatial geometries. Afterward, the EOF model of Sq current function was reconstructed using the first three eigenmodes, which captured 96% of the overall variance. Several patterns of the Sq current were uncovered, addressing some unanswered questions about the dominant mechanisms that drive their spatial, seasonal and inter-annual variability. This study suggests that the dynamics of Sq current variability can be conveyed by a few dominating eigenmodes, indicating that our model could well capture the Sq current variability and serve as a new observational baseline for further development of geomagnetic field models.

1. Introduction

External forcing by energetic solar radiation such as extreme ultraviolet (EUV) irradiance and waves forcing from the lower atmosphere drive the ionospheric variations via multiple ways, including the solar ionization variability caused by the 11-year solar cycle and 27-day solar rotation. The forcing of the ionosphere by waves from below is mostly created by neutral atmospheric waves, such as gravity and planetary waves (e.g., Laštovička, 2006). These complex variations influence the ionospheric conductivity, which in turn impact the electric fields generated by the dynamo action of tidal winds in the ionosphere, and hence the solar quiet (Sq) current variation induced in the ionospheric E-region (e.g., Richmond, 1998; Weimer, 2005, 2013; Yamazaki et al., 2011, 2016). In the middle

and low latitude ionosphere, large-scale magnetospheric processes such the field aligned current (FAC) system also contribute to Sq current variation (e.g., Vanhamäki et al., 2020; Yamashita & Iyemori, 2002).

The morphology of the Sq current variation appears like oval-shaped horizontal current sheet in the ionosphere, forming two oppositely oriented loops on the dayside in each hemisphere: one anticlockwise in the northern hemisphere (NH) and one clockwise in the southern hemisphere (SH), with the foci of the loops located near noon in the middle latitudes (e.g., Owolabi et al., 2021; Pedatella et al., 2011; Richmond, 1998; Yamazaki et al., 2011). At the geomagnetic equator, where ions and electrons are magnetically coupled, the electric and magnetic fields intersect, resulting in a local increase in ionospheric conductivities and a large eastward flow of equatorial electrojet (EEJ) current during the daytime (e.g., Alken & Maus, 2007). On occasion, during geomagnetically quiet periods, the EEJ current reverses its regular eastward course and flows westward due to changes in the atmospheric tides that govern the global wind system at the ionospheric E-region; this phenomenon is referred to as counter electrojet (CEJ) current (e.g., Soares et al., 2018).

Earlier studies based on various observations and modeling techniques, particularly those pertaining to empirical curve fitting of Sq current variation have been conducted (e.g., S. S. Chen et al., 2020, 2021; Vanhamäki et al., 2020; Yamazaki et al., 2009, 2010, 2011). These studies explored the dynamics of the ionosphere and its interaction with the magnetosphere, in particular, examining the consequences of universal time (UT), season and day-to-day variations (e.g., S. S. Chen et al., 2021; Kirchhoff & Carpenter, 1976; Pfaff et al., 2020; Schlapp & Butcher, 1995; Yamazaki et al., 2016), including the effects of local neutral winds (e.g., Maute, 2017; Yamazaki et al., 2021). It was remarked that due to variations in the ionospheric conductivity and neutral winds, the Sq current system exhibits hemispheric asymmetry, with its strength in the summer hemisphere being greater than that in the winter hemisphere. A large number of studies have been devoted in understanding the seasonal and solar activity variations of the Sq current (e.g., Matsushita & Maeda, 1965; Owolabi et al., 2021; Takeda, 2002; Takeda et al., 1986). For example, Yamazaki et al. (2011) found strong annual and semiannual changes of the Sq current in the northern and southern hemispheres, which Pedatella et al. (2011) also found in the European/African sector during solar minimum. A recent study by Chulliat et al. (2016) indicates a wave-4 structure in the longitudinal variation of total Sq current (J_{total}) intensity under high solar activity conditions having implications on seasonal variation, where the largest J_{total} is found in the equinox rather than in the winter season.

In addition, the solar cycle variability of the Sq current can be explained using an empirical orthogonal function (EOF) analysis that uses empirical orthogonal windows to estimate the major spatial and temporal patterns that do not require a priori specification of their geometry (e.g., Alken et al., 2017; G.-X. Chen et al., 2007; Cousins et al., 2015; Shore et al., 2016). This empirical model is appropriate for geomagnetic field modeling since it decomposes the signal into uncorrelated eigenmodes, resulting in eigenfunction expansion used to probe the time-varying Sq current (e.g., Alken et al., 2017; Owolabi et al., 2021). Different sources have been proposed for Sq current variations, including long-term variation in geomagnetic activity (e.g., de Haro Barbas et al., 2013), solar variability (e.g., Torta et al., 2009) and the secular variation of the geomagnetic field (e.g., Cnossen & Richmond, 2013; Soares et al., 2020). Since the Sq current conceals seasonal and non-seasonal effects in the underlying background variations that are still not well understood, EOF analysis can give a set of dominant eigenmodes that collectively identify patterns in Sq current system, which reflect the underlying background variations modulating the original signature. The EOF model of the Sq current by G.-X. Chen et al. (2007) captured the key aspects of the geomagnetic field variations, especially the horizontal field intensity (e.g., Alberti et al., 2020; Bhattacharyya & Okpala, 2015). A study by Alken et al. (2017) demonstrated that their EOF model reproduces realistic Sq and EEJ currents by utilizing 10 dominating eigenmodes.

As described by Shore et al. (2018), the EOF analysis was used to decompose the monthly geomagnetic field data into a hierarchy of spatial and temporal patterns. The leading eigenmodes were related to Sq current variations, while the residual eigenmodes encompassed disturbance polar (DP) currents, which are associated with the magnetospheric ring currents (e.g., Xu & Kamide, 2004). Based on the EOF analysis, Yamada (2009) demonstrated that dynamo activity drives electric fields and currents in the ionosphere. Until now, the spatial distribution of the Sq current based on the EOF analysis for different solar activity levels has not been well studied. A study by Pedatella et al. (2011) produced the Sq current pattern to highlight the mechanism for the seasonal and longitudinal variations during the low solar activity years. The Sq current pattern during high solar activity needs to be identified due to its latitudinal and longitudinal dependency. We utilized ground magnetometer data from 2006 - 2019 to produce continuous observations of the Sq current function using spherical harmonic analysis (SHA)

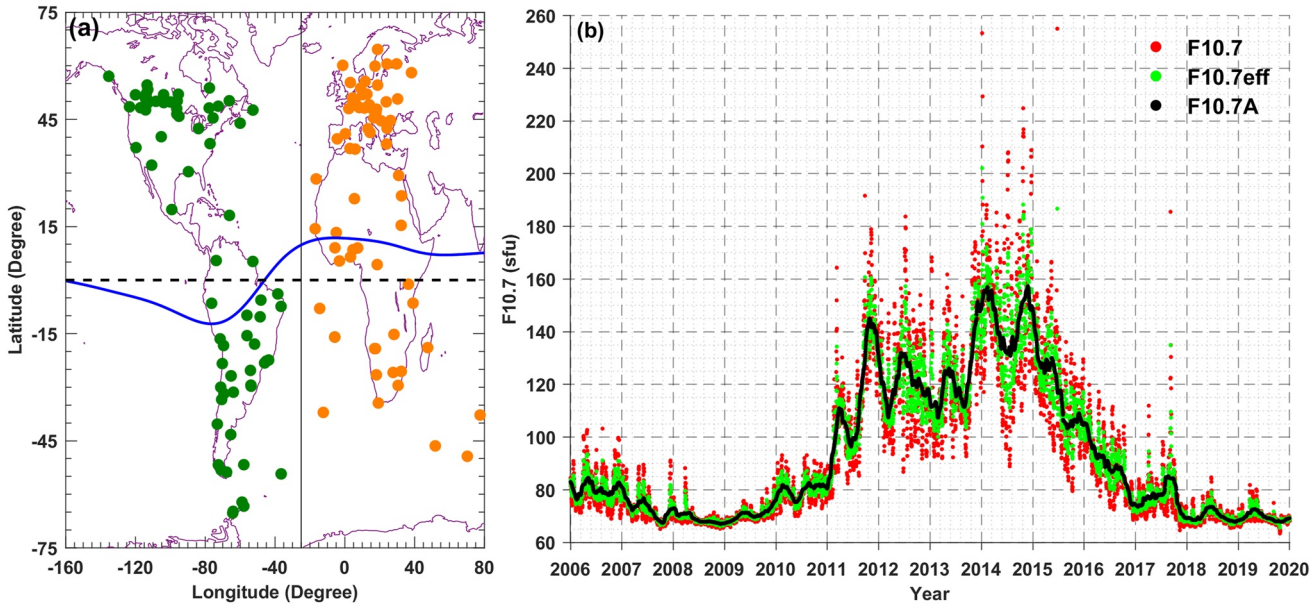

Figure 1. (a) Geographic location of 125 geomagnetic observatories used in this study. The green and orange dots represent magnetometer stations located over the American and European/African sectors, respectively. The geomagnetic and geographic equators are indicated by the blue curve and dashed black line. (b) Solar activity proxy, F10.7 flux (red dots), its 81-day moving average, F10.7A (black dots) and effective solar flux, $F10.7_{\text{eff}}$ (green line) from 2006 to 2019. The $F10.7_{\text{eff}}$ is obtained by taking the mean of F10.7 flux with F10.7A. The vertical gray lines represent the end of each year.

and examine its spatial as well as temporal variations under different solar activity levels over the American and European/African sectors. Subsequently, the EOF technique was used to reconstruct a two-dimensional (2-D) model of the Sq current under certain condition of solar flux, magnetic latitude, local time and season over the two longitudinal sectors using the dominant spatial geometries, as the EOF technique has been noticeably effective in characterizing the spatial and temporal variations (e.g., Alberti et al., 2020; Alken et al., 2017; Owolabi et al., 2021). First, we have attempted to find the similarities as well as differences in the spatial and temporal variations of the Sq current. Then we studied the distribution of the typical parameters of the Sq current over the two longitudinal sectors and discussed the source of their differences under different solar activity levels.

2. Data Selection and Method of Analysis

2.1. Geomagnetic Field and Solar Flux Data

Hourly data of horizontal intensity (H), declination (D), and vertical intensity (Z) obtained from 2006 to 2019 were evaluated for Sq geomagnetic variations. The ground magnetometer data were collected from 125 stations spread across the American and European/African sectors, which were operated by the Athabasca University Themis UCLA Magnetometer Network (AUTUMNX); MAGnetic Data Acquisition/Circum-pan Pacific Magnetometer Network (MAGDAS/CPMN; Yumoto & the MAGDAS Group, 2006); Low Latitude Ionospheric Sensor Network (LISN); African Meridian B-Field Education and Research (AMBER; Yizengaw & Moldwin, 2009); International Real-time Magnetic Observatory Network (INTERMAGNET; Kerridge, 2001); Embrace Magnetometer Network (Embrace MagNet; Denardini et al., 2018); Canadian Array for Realtime Investigations of Magnetic Activity (CARISMA; Mann et al., 2008); South American Meridional B-Field Array (SAMBA; Boudouridis & Zesta, 2007); West African Magnetometer Network (WAMNET; Alken et al., 2013); and World Data Center for Geomagnetism (WDC), Edinburgh (Figure 1a). We obtained 5 International Quiet Days (IQDs) data from the Helmholtz Center Potsdam, German Research Center for Geosciences GFZ webpage. To analyze the Sq current variations, the F10.7 flux data in solar flux units (sfu), 1 sfu = 10^{-22} Wm^{-2} Hz^{-1}, were obtained from the GSFC/SPDF OMNIWeb interface. The quasi-magnetic latitude was computed using the main field model (IGRF-2013 version) at the epoch of 2015 provided by the International Association of Geomagnetism and Aeronomy (IAGA).

2.2. Basis of SHA and Sq Current Computation

For each station, H, D and Z components are selected from the geomagnetic field records based on 5 IQDs for every month from 2006 to 2019. This condition gives a total of 840 IQDs, which has been found to be satisfactory and forms the database used to derive the Sq geomagnetic variations. To resolve the spatial complexities of the Sq current variation, the records of H, D and Z components outside $3° < |\theta| \leq 60°$ geomagnetic latitudes are excluded from the analysis. Here, θ is the geomagnetic latitude. Next, we obtained the hourly average of ΔH, ΔD and ΔZ components by deducting the baseline values of H, D and Z at LT ≤ 2 or LT ≥ 23 from the corresponding component (LT = local time in hours). Then, SHA is performed on ΔH, ΔD and ΔZ components at each geomagnetic colatitude based on dominant harmonics rank m in the range $0 \leq m \leq 4$ to calculate the spherical harmonic coefficients. Consequently, the Sq current functions over the two longitudinal sectors were obtained for each IQD at every hour of LT and geomagnetic colatitude, respectively based on Equation 1 (e.g., Owolabi et al., 2021; Yamazaki & Maute, 2017).

$$J(t,\theta) = -\frac{10R}{4\pi}\sum_{n=m}^{m+9}\sum_{m=0}^{n}\frac{2n+1}{n+1}\left(\frac{r}{R}\right)^{n}\left\{E_n^m\cos(mt) + e_n^m\sin(mt)\right\}P_n^m(\cos\varphi) \tag{1}$$

where $r = R$ is assumed in the calculations because $|r - R| \ll R$, $P_n^m(\cos\ \varphi)$ is the associated Legendre function of geomagnetic colatitude, n and m are the degree and order at which the series of harmonics function is truncated, $R = 6{,}371$ km is the Earth's radius, r is the radius vector from the center of the Earth, t is the LT in hours, and φ is the geomagnetic colatitude of the observatory obtained by $\varphi = 90 - \theta$. We chose $n = 4$ as the maximum spherical harmonic expansion to eliminate larger errors caused by higher harmonic terms and to resolve the large-scale structure of the Sq current variation (e.g., Takeda, 1999). The E_n^m and e_n^m are empirical constants denoting the Gaussian coefficients, whose sources are external to the Earth.

2.3. Description of EOF Analysis and Modeling Algorithm

In this study, the EOF eigenmodes are obtained by solving the eigenvalue problem based on the Eigen decomposition theorem. We constructed a 2-D model of $J(t,\theta)$ function for different solar activity levels to identify coherent quantities extracted (as in Equation 2), which are relevant to the phenomenon of $J(t,\theta)$ function over the two longitudinal sectors. We considered the leading eigenmodes in reconstructing the 2-D model of $J(t,\theta)$ function because they provide an efficient basis for expressing the Sq current function and are also optimal in the least squares sense. This is due to the orthonormality of the eigenvectors and the magnitude ordering of the eigenvalues that indicates the significance of each term in the expansion. This phenomenon clearly demonstrates the advantage of the EOF modeling approach proposed in this paper. The data set may be represented as 2-D matrix $J'(d,x)$ in Equation 2.

$$J'(d,x) = \sum_{k=1}^{q}\mathrm{Amp}_k\ (d) * \mathrm{EOF}_k(x) \quad k = 1,2,3...,q \tag{2}$$

where EOF_k represents an orthogonal function independent of time, Amp_k is the time-dependent principal component (PC) amplitude of each EOF eigenmode, k varies from 1 to the maximum number of eigenmodes (q) contained in the Sq current function, with eigenmodes arranged in order of decreasing variance, $d = 1, 2, 3\ldots$, 840 is the number of IQDs from January 2006 to December 2019, $x = 1, 2, 3, \ldots, s$ (s = station × 24) denotes spatial positions or basis functions in certain order of stations and LT. It is important to know that the dimension that we sum over gives q × q product matrix with q eigenmodes, where q equals 1632 and 1368 eigenmodes in the American (68 stations × 24) and European/African (57 stations × 24) sectors, respectively. The first three EOF eigenmodes capture 96% of the overall variance and statistically significant, with the residual EOF eigenmodes contributing only 4%-a difference that is statistically insignificant (e.g., Owolabi et al., 2021). It is evident that the first three EOF eigenmodes are significant because their eigenvalues are well separated. Therefore, we focus on the first three eigenmodes. Regression analysis is performed to reconstruct the Sq current dynamics by fitting the annual, semiannual, and terannual changes in Amp_k ($k = 1, 2, 3$) since its seasonal variation has annual, semiannual and terannual components influenced by solar activity variations.

$$\left.\begin{aligned} \mathrm{Amp}_k(d) &= A_s * R_s \\ A_s &= a_o + a_1 * F10.7p + a_2 * F10.7_{\mathrm{eff}} \\ R_s &= c_0 + \sum_{k=1}^{3}\left(p_k \cos\left(\frac{2\pi * \mathrm{DOY} * k}{365.25}\right) + q_k \sin\left(\frac{2\pi * \mathrm{DOY} * k}{365.25}\right)\right) \end{aligned}\right\} \quad (3)$$

where $c_0$is the mean value of EOF eigenmodes over the entire series, leap years were accounted for by adding a 0.25-factor to the 365-day calculation, $F10.7p$ is the F10.7 flux of the previous day, $F10.7_{\mathrm{eff}}$ = (F10.7 + F10.7A)/2, F10.7A is the 81-day sliding mean of daily F10.7 flux and DOY is the date number from January 1 of each year for the quiet days, which all depends on solar activity. Using $F10.7_{\mathrm{eff}}$, previous studies have shown that most solar EUV flux lines can be correctly scaled to incorporate solar cycle variation. As shown by Liu et al. (2006), $F10.7_{\mathrm{eff}}$ can better present the variations of solar EUV irradiance since the nonlinearity of the solar EUV flux is reduced and the correlation is slightly stronger with $F10.7_{\mathrm{eff}}$. Hence, we used the $F10.7_{\mathrm{eff}}$ as a reliable proxy for solar activity variation to fit the EOF model on individual days and LT (e.g., Richards et al., 1994). As shown in Figure 1b, the F10.7 flux, which represents the degree of solar activity, exhibits variation throughout a 14-year period of study. The first three parameterized eigenmodes in the American (European/African) sectors have a regression coefficient of 0.76 (0.78), 0.90 (0.94) and 0.60 (0.44) with PC amplitudes, respectively (Figures 2 and 3). The time series of the Sq current parameters such as the northern Sq intensity, southern Sq intensity and J_{total} from the two longitudinal sectors were obtained under high ($F10.7_{\mathrm{eff}} = 160$ sfu), moderate ($F10.7_{\mathrm{eff}} = 120$ sfu) and low ($F10.7_{\mathrm{eff}} = 80$ sfu) solar activity levels, respectively.

3. Observational Results and Discussion

Based on the EOF analysis described in Section 2.3, an EOF model is developed to identify and extract the spatial and temporal variability prevailing in the Sq current function for different solar activity conditions over the American and European/African sectors. Figures 2 and 3a–3c display the first three EOF eigenmodes of the Sq current variations as a function of geomagnetic latitude and LT from 2006 to 2019 over the two longitudinal sectors. Their corresponding time-dependent PC amplitudes are also shown in Figures 2 and 3d–3f. In the higher eigenmodes, large-scale magnetospheric currents such as the cross-tail current, the ring current, magnetopause current as well as unresolvable partial ring current may be present (e.g., Xu & Kamide, 2004), hence the higher EOF eigenmodes will not be discussed in this study. We observed that PC1 is significantly dependent on solar activity, while PC2 and PC3 are not strongly dependent on solar activity, but they do have significant annual, semiannual and interannual oscillations with varied amplitudes. As shown in Figures 2a and 3a, the EOF1 eigenmode of Sq current over the two longitudinal sectors exhibits similar pattern with their intense vortices on the sunlit side in both hemispheres, which confirms the daily variation of ionospheric conductivities (e.g., Pedatella et al., 2011; Yamazaki et al., 2011).

Certain interesting features emerge from Figures 2b and 3b. In particular, the EOF2 eigenmode pattern is characterized by the meridional currents across the magnetic equator in the morning sector and oppositely directed currents in the afternoon sector. The EOF3 eigenmode is also characterized by meridional currents across the magnetic equator, but the maximum current appears around the noon sector (Figures 2c and 3c). When comparing the EOF2 eigenmode in both longitudinal sectors, the most important distinction is that their peak locations are different; one is in the northern hemisphere while the other one is in the southern hemisphere. As seen in Figure 1a, in the American sector, the magnetic equator is mainly in the SH, while in the European/African sector, it is mainly in the NH. Thus, for example, equatorial winds drive NH Sq currents in the American sector, while they drive SH Sq currents in the European/African sector. These apparent imbalances appear to be the result of many variables, including ionospheric conductivity, geomagnetic field, and neutral winds (e.g., Campbell, 1981; Stening, 1991). Over the American sector, the SAMA-induced deviation in the geomagnetic equator alters the Pedersen and Hall conductivities, giving larger ionospheric conductivity distributions for a weaker magnetic field, causing the longitudinal variation in the Sq current. A detailed account of the seasonal and longitudinal variations of the Sq current can be found in several previous publications (e.g., Pedatella et al., 2011; Stening, 1971; Stening & Winch, 2013). The geomagnetic equator declination angle is about −20° over the eastern coast of South America. Such a high magnetic declination affects the seasonal distribution of EEJ and Sq currents (e.g.,

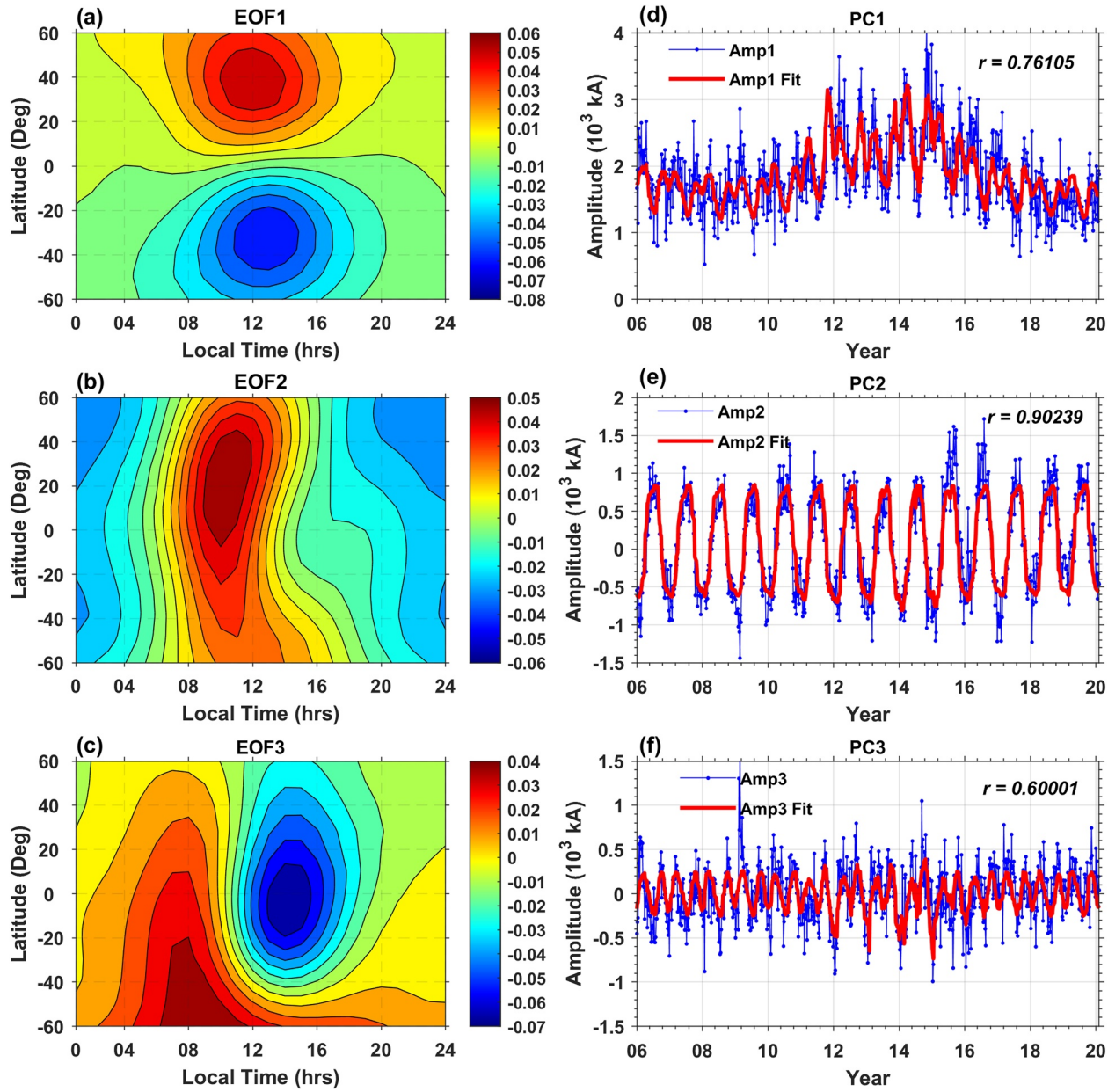

Figure 2. Spatial and temporal variations for eigenmodes 1–3 of the empirical orthogonal function (EOF) analysis of the Sq current in the American sector. (a) EOF1 eigenmode with a contour interval of 0.01. Also shown are (b) EOF2 and (c) EOF3 eigenmodes. The amplitudes of their corresponding principal components (PC1-PC3) are shown in panels (d–f), respectively. The regression coefficients (r) are shown in each panel.

Abdu et al., 2005; Shume et al., 2010). Another important factor is the day-to-day changes in the neutral wind and electric fields, which could vary greatly between longitudinal sectors and influence the dynamo electric fields and currents. For both sectors, the overall LT-latitude patterns of the EOF2-EOF3 eigenmodes, which serve as regional patterns of annual and semiannual oscillations exhibit sunrise and sunset variations.

It is important to know that the combination of the first three EOF eigenmodes and their PCs results in the Sq current variations shown in Figures 4a and 4b, respectively. In this Figure, the Sq current flows parallel to the streamlines with 20kA between each line. On the sunlit side, a well-defined anticlockwise current vortex in the NH and a clockwise current vortex in the SH of American sector. The Sq current vortex is higher in the SH and lower in the NH, where the NH vortex actually leads the SH vortex by nearly 0.8 hr with a mean focus located at about ±40° magnetic latitude (Figures 2a and 4a). The north-south asymmetry of the geomagnetic field can contribute to the

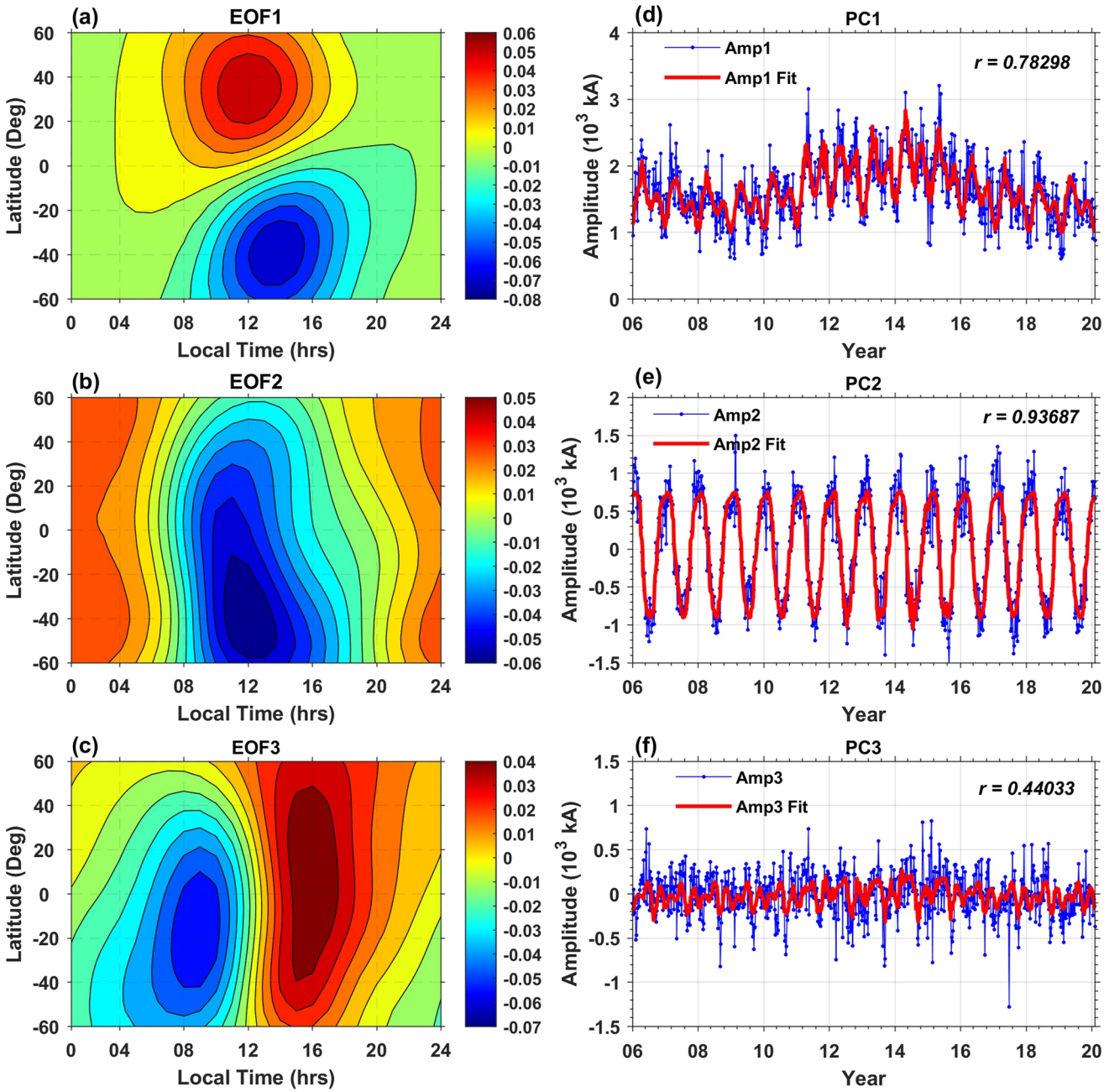

Figure 3. Similar to Figure 2 except for the European/African sector.

LT displacement of the Sq current vortices (e.g., Le Sager & Huang, 2002; Takeda & Yamada, 1989). Likewise, over the European/African sector, the LT separation of both vortices is about 2.5 hr with the mean focus located at about ±38° magnetic latitude (Figures 3a and 4b). This is consistent with previous work reported in the East Asian/Australian sector (e.g., Yamazaki et al., 2011). Comparing Figures 4a and 4b, we notice that the northern current vortex expels into the SH in the morning sector and the southern current vortex penetrates less intensely into the NH in the afternoon sector (e.g., Fukushima, 1994). Such a deep cross-equatorial Sq current flow is not evident in the American sector (Figure 4a). The causes of the deep penetration of the northern current vortex into SH in the morning sector and vice versa in the afternoon sector over European/African sector need further study. Although, studies have shown that cross-equatorial current is partially generated by inter-hemispheric FAC system (e.g., Richmond & Roble, 1987; Takeda, 1990; Yamashita & Iyemori, 2002). The intensity and direction

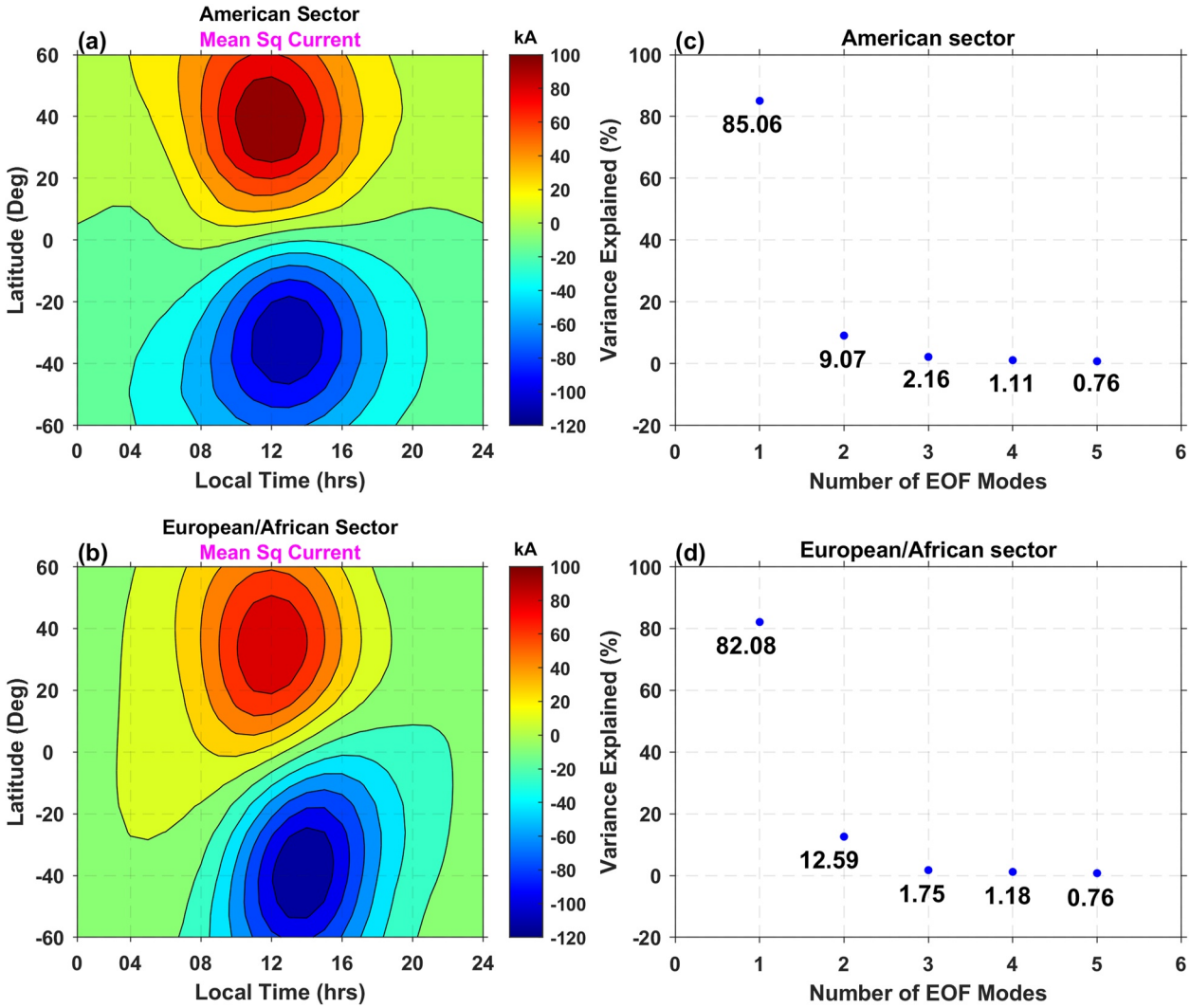

Figure 4. The Sq current average from 2006 to 2019 over the American and European/African sectors are shown in panels (a and b), respectively. The corresponding percentage of variance explained accounted for by each of the first 5 most eigenmodes are shown in panels (c and d), respectively. The index number of the empirical orthogonal function (EOF) eigenmodes, where the first EOF eigenmode is well separated from the rest is ordered from largest to smallest.

of the inter-hemispheric FAC system vary with the longitude (e.g., Park et al., 2011, 2020), which can contribute to the difference in the north-south asymmetry of the Sq current system between the two longitudinal sectors.

As illustrated in Figure 4 (panels c and d), the first three EOF eigenmodes, which show the contribution of each latent factor to the Sq current variation over the American (European/African) sector, take up 85.06% (82.08%), 9.07% (12.59%) and 2.16% (1.75%) of the total variance of the Sq current, respectively. The PCs corresponding to EOF2 and EOF3 eigenmodes exhibit an oscillation around zero as shown in panels (e and f) of Figures 2 and 3, respectively. When a PC value is negative, clockwise/anticlockwise current vortices (panels (b–c) of Figures 2 and 3) will change to anticlockwise/clockwise vortices, respectively. It can be seen in Figures 2d and 3d that PC1 exhibits seasonal variation and is dependent on solar activity (Figure 1b), while PC2 and PC3 exhibit annual and interannual variations, respectively (panels (e–f) of Figures 2 and 3). The temporal behavior of EOF1 eigenmodes (Figures 2d and 3d) demonstrates a relatively strong dependence on solar activity. As can be seen, the EOF eigenmodes are distinct in both longitudinal sectors, particularly for the EOF2 and EOF3 eigenmodes, which may be explained by the offset of the magnetic equator with respect to the geographic equator. In principle, the spatial and temporal patterns of the Sq current over the American (Figure 2) and European/African sectors (Figure 3) retain 96% of the total Sq current variance, suggesting that the temporal evolution of the dynamical interaction represents periodic behavior of Sq current variations. The first three eigenmodes describe the effects

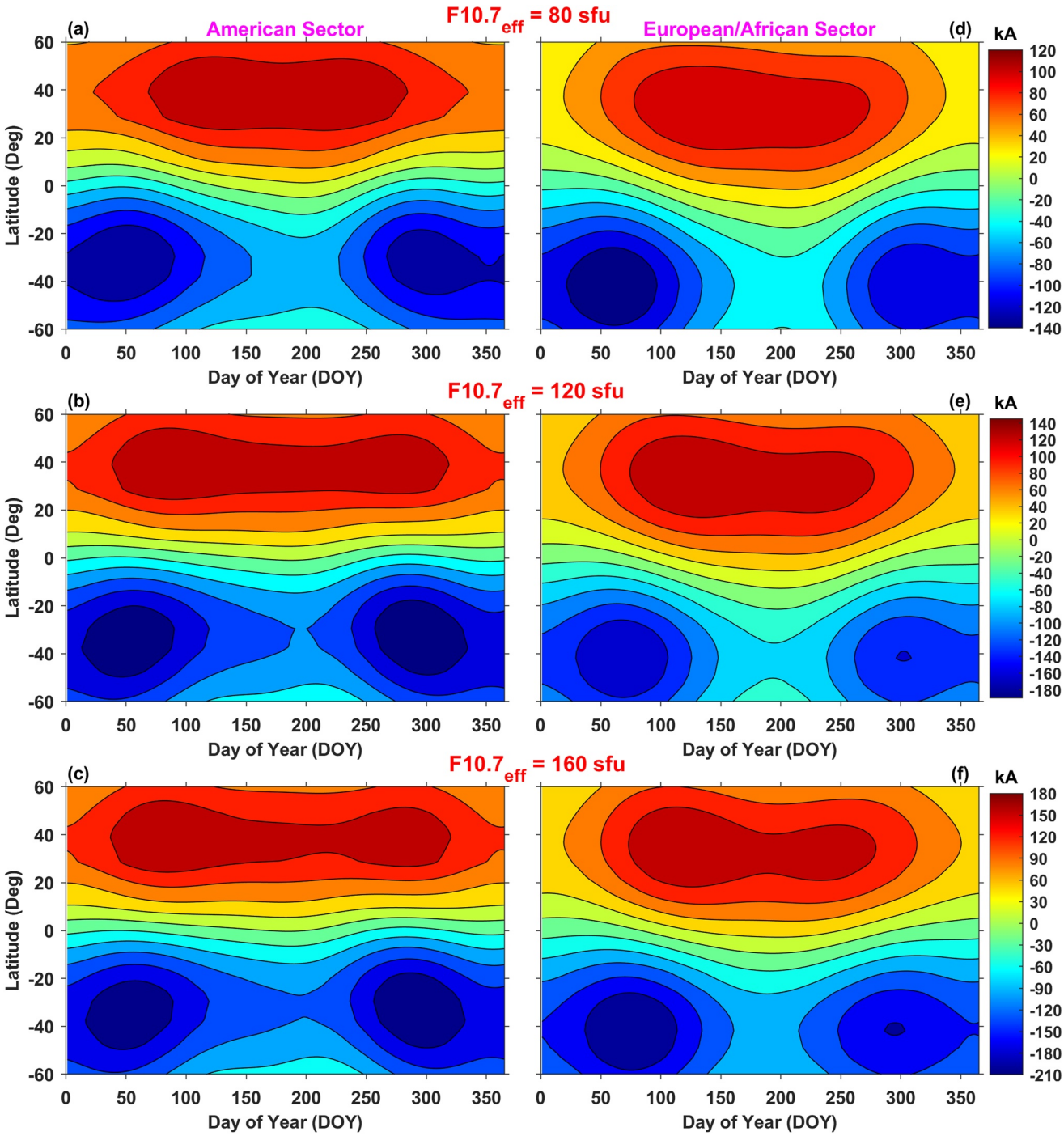

Figure 5. Seasonal variation of Sq current at 12:00 LT derived from the empirical orthogonal function model under different solar activity conditions as indicated on the panels. (a–c) Sq current variation obtained over the American sector. (d–f) Same as panels (a–c) except for the European/African sector.

on the geomagnetic field of the Sq ionospheric current. The residual, which indicates the long-term trend of the Sq current is attributed to the magnetospheric ring current (e.g., Xu & Kamide, 2004). Thus, the EOF model of Sq current can help in the understanding of the external magnetic field variations.

As the Sq current depends strongly on solar activity and consequent solar cycle variation, we obtain the Sq current at 12:00 LT for minimum ($F10.7_{\text{eff}} = 80$ sfu) moderate ($F10.7_{\text{eff}} = 120$ sfu) and maximum ($F10.7_{\text{eff}} = 160$ sfu) solar conditions as shown in Figure 5. Under solar minimum conditions, the northern Sq current has a June

solstice peak and the weakest at the December solstice, with some intermediate values at the Equinox, while the southern Sq current exhibits a semiannual variation with a peak around the Equinoctial months and weakest in the solstitial months. For moderate solar activity, the northern and southern current intensities exhibit annual and semiannual variations in the northern and southern hemispheres, respectively, that is, the amplitude of the northern current intensity peaks in June solstice while the amplitude of the southern current intensities increases the Equinox. Under solar maximum conditions, the NH Sq current also shows a semiannual variation, which is especially evident in the American sector. In low and equatorial latitudes, the weakest magnitude appears at the June solstice, but the magnitude of the December solstice is not the weakest. At middle latitudes, the annual variation appears to be clearer than the semiannual component. The annual variation is associated with the Sq amplitude being greater during summer than winter at middle latitudes, whereas the semiannual component is typically associated with the Sq amplitude being greater during equinoctial months than other times at low and equatorial latitudes (Pedatella et al., 2011; Yamazaki & Maute, 2017). As expected, displayed high value of the Sq current in the American sector, and its temporal distribution obviously differs across the two longitudinal sectors, further confirming the longitudinal differences of the geomagnetic Sq field (e.g., Pedatella et al., 2011). Several other confounding factors may contribute to the observed spatial and temporal variability of Sq current. The effects of hemispheric conductivity differences on Sq current and resultant magnetic field perturbations have been explored extensively (e.g., Pedatella et al., 2011). In both hemispheres, seasonal variations in thermospheric wind patterns and ionization levels are considered to be responsible for these properties (e.g., Yamazaki et al., 2011).

Earlier, Campbell and Matsushita (1982) compared the seasonal variation of the NH Sq current in the American sector during the solar minimum year of 1964 and the solar maximum year of 1958, respectively. They noted that the Sq current exhibited an annual variation in 1964 but a semiannual variation in 1958. The enhanced/reduced semiannual variation of the NH Sq current under solar maximum/minimum conditions is consistent with our results. The Sq current asymmetry is more pronounced in the European/African sector compared with the American sector. The prevailing northern annual variation that peaks in the June solstice can be attributed to a higher conductivity caused by increased insolation in the dynamo region during the June solstice, which results in stronger Sq current during this period (e.g., Pedatella et al., 2011; Takeda, 1999, 2002). At $F10.7_{\text{eff}} = 160$ sfu, the Sq current at 12:00 LT exhibits semiannual variation in both hemispheres, and the intensities in equinoxes are much greater than in solstices (e.g., Takeda, 2002; Yamazaki et al., 2011).

Solar activity dependence of the Sq current parameters such as the northern Sq current intensity, southern Sq intensity and J_{total} over the two longitudinal sectors are depicted in Figure 6. In this Figure, we observed that J_{total} defined as the total currents flowing in the dayside vortex in each hemisphere has a clear dependence on the location, season, solar activity levels with greater peaks in equinoxes over the two longitudinal sectors. For example, there is a significant seasonal asymmetry between the equinox and solstice despite a similar amount of heating coming from the Sun in both longitudinal sectors (e.g., Chulliat et al., 2005). This demonstrates that the dominant tidal winds responsible for the J_{total} is at their strongest at the equinoxes. Possible physical mechanism is the semiannual variation of the Sq current resulting from the diurnal wind semiannual change (e.g., Yamazaki et al., 2009). Pedatella et al. (2011) pointed out that the seasonal and longitudinal variations of the Sq current exhibit amplitude modulations which appear to be related to the influence of nonmigrating tides. Such a behavior is largely due to the geomagnetic main field effects caused by ionospheric conductivity differences and the offset between the geographic and geomagnetic equators (e.g., Takeda, 1999; Yamazaki et al., 2011). In addition, the northern Sq current changes semiannually, which is most pronounced during high solar activity ($F10.7_{\text{eff}} = 160$ sfu) with peaks in April and October (Figure 6b), agreeing with prior research (e.g., Takeda, 1999). The equinoctial peaks of the J_{total} intensity is also evident during the moderate solar activity ($F10.7_{\text{eff}} = 120$ sfu). The pattern is similar to that observed during the high solar activity ($F10.7_{\text{eff}} = 160$ sfu), except that the slight change in magnitude. For $F10.7_{\text{eff}} = 80$ sfu, the northern Sq current intensity shows annual variation with peak around the solstices in both longitudinal sectors.

In Figure 5c, and a strong semiannual variation in the southern Sq current intensity is observed in both longitudinal sectors with maximum value in the solstice, and an annual variation with maximum values near the solstice during the moderate and low solar activity conditions. Similar variations in the amplitude of J_{total} with solar activity levels has been reported in the Asian/Australian sector (e.g., Yamazaki et al., 2011). Thus, the details of the solar cycle as well as seasonal analyses of J_{total} differ longitudinally (e.g., Pedatella et al., 2011). Previous studies have suggested that the semiannual change of Sq currents can be explained by the seasonal variation of migrating

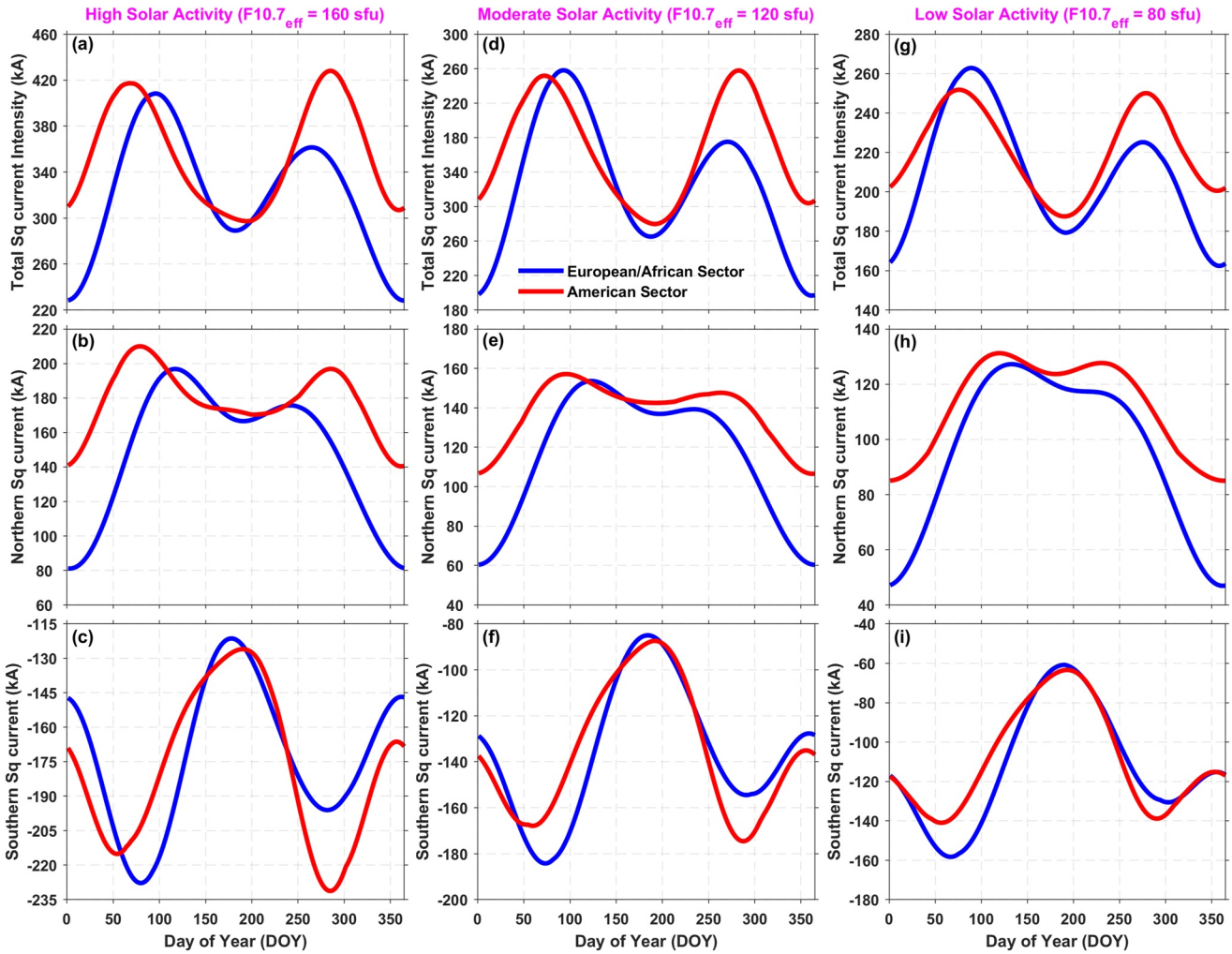

Figure 6. Seasonal variation of the averaged Sq current parameters derived from the empirical orthogonal function model in the American sector (red line) and European/African sector (blue line) during high (left), moderate (middle) and low (right) solar activity levels. The first-row panels show the total Sq current intensity. The second and third row panels represent the northern and southern current intensities, respectively.

tides (e.g., Yamazaki & Maute, 2017). Overall, our results suggest that the EOF approach could capture patterns of spatial and temporal variability of Sq current function by extracting distinct patterns in the Sq current function. This mathematical technique could help discover how external solar forcing is reflected in the ionosphere. Extending the EOF investigation to long-term global geomagnetic field data could help understand the longitudinal structure and physical mechanisms involved.

4. Conclusion

We have constructed an EOF model of Sq current function under different solar activity conditions based on the ground magnetometer data over the American and European/African sectors for the years 2006–2019. The EOF model, which captured 96% of the total Sq current variance, is characterized by large-scale spatial and temporal patterns. The EOF model reconstruction unveils a significant dependence of the Sq current on solar activity, magnetic latitude, local time and season, suggesting a contribution from the EUV, and ionosphere-thermosphere coupling. In both longitudinal sectors, similar Sq current patterns were present under different solar activity conditions, although we observed some differences in their Sq current amplitudes. Besides, the newly developed model could reproduce a refined Sq current variability over the two longitudinal sectors as long as the observed Sq variation data have sufficient duration, which could help in assessing the space weather effects. However, this model only accounts for the influence of solar activity, season, magnetic latitude and local time over the

two longitudinal sectors, while there exist other driven sources requiring further investigation. In effect, a more detailed study would be required using space-ground conjugate magnetometer observations to further elucidate the large-scale Sq current variation and dynamics in relation to solar activity conditions. This understanding is necessary for effective prediction of the Sq current variations, and efforts are underway to fully characterize how the longitudinal structure of the Sq current system varies with solar activity.

Data Availability Statement

This study utilizes ground magnetometer data from various sources, including the LISN (http://lisn.igp.gob.pe/jdata/database/), AMBER (http://magnetometers.bc.edu/index.php/downloads), INTERMAGNET (https://www.intermagnet.org/data-donnee/download-eng.php) AUTUMNX (http://autumn.athabascau.ca/magdata/L1/), WDC (http://www.wdc.bgs.ac.uk/catalog/master.html), CARISMA (http://www.carisma.ca/carisma-data-repository), SAMBA (http://magnetometers.bc.edu/index.php/downloads), EMBRACE (http://www2.inpe.br/climaespacial/SpaceWeatherDataShare/), WAMNET (http://www.bcmt.fr/wamnetnetwork.html) and MAGDAS/CPMN networks. The MAGDAS/CPMN geomagnetic data are available upon request from Dr. Akimasa Yoshikawa at the International Center for Space Weather Science and Education, Kyushu University, Fukuoka, Japan (yoshi@geo.kyushu-u.ac.jp). The geomagnetic coordinates are calculated through the IAGA website's quasi dipole coordinate calculator (http://www.geomag.bgs.ac.uk/data_service/models_compass/coord_calc.html). The F10.7 flux and Kp indices are archived on the NASA Goddard Space Flight Center's SPDF/GSFC website (https://omniweb.gsfc.nasa.gov/form/dx1.html). The Helmholtz Center Potsdam in Germany, known as the GFZ, collects and stores records on the IQDs (https://www.gfz-potsdam.de/Kp-index/).

Acknowledgments
The first author is indebted to Prof. Jiuhou Lei for his guidance over the years in the pursuit of understanding the ionospheric electrodynamics and to Prof. Yufeng Lin for his support and encouragement during this work. This work was supported by the National Natural Science Foundation (NSF) of China (Grant numbers: 41804151 & 42074186), and Natural Science Foundation of Jiangsu Province (Grant Number: BK20211036). The authors are thankful to the LISN, AMBER, INTERMAGNET, AUTUMNX, WDC, CARISMA, SAMBA, EMBRACE, MAGDAS/CPMN and WAMNET members for providing the geomagnetic data used in this study. The LISN is a project led by Boston College in collaboration with the Geophysical Institute of Peru, and other institutions that provide information for the benefit of the scientific community. The AMBER is operated by Boston College and funded by NASA and AFOSR. The CARISMA network is operated by the University of Alberta, funded by the Canadian Space Agency. The SAMBA is also operated by UCLA and funded by NSF. The AUTUMNX is funded through the Canadian Space Agency/Geospace Observatories (GO) Canada Program. The MAGDAS/CPMN network is operated by the International Center for Space Weather Science and Education, Kyushu University, Fukuoka, Japan and funded by the Japan Society for the Promotion of Science (JSPS). The authors appreciate the IAGA for providing a quasi-dipole geomagnetic coordinate calculator. The authors are very grateful to SPDF/GSFC for providing records of F10.7 flux indices used in the present study. The authors thank the Helmholtz Center Potsdam, German Research Center for Geosciences GFZ for providing records of the IQDs. The authors thank the editor and two anonymous reviewers for their helpful comments and suggestions that greatly improved this paper.

References

Abdu, M. A., Batista, I. S., Carrasco, A. J., & Brum, C. G. M. (2005). South Atlantic magnetic anomaly ionization: A review and a new focus on electrodynamic effects in the equatorial ionosphere. *Journal of Atmospheric and Solar-Terrestrial Physics*, *67*(17-18), 1643–1657. https://doi.org/10.1016/j.jastp.2005.01.014

Alberti, T., Giannattasio, F., De Michelis, P., & Consolini, G. (2020). Linear versus nonlinear methods for detecting magnetospheric and ionospheric current systems patterns. *Earth and Space Science*, *7*, e2019EA000559. https://doi.org/10.1029/2019EA000559

Alken, P., Chulliat, A., & Maus, S. (2013). Longitudinal and seasonal structure of the ionospheric equatorial electric field. *Journal of Geophysical Research: Space Physics*, *118*, 1298–1305. https://doi.org/10.1029/2012JA018314

Alken, P., & Maus, S. (2007). Spatio-temporal characterization of the equatorial electrojet from CHAMP, Ørsted, and SAC-C satellite magnetic measurements. *Journal of Geophysical Research*, *112*. https://doi.org/10.1029/2007JA012524

Alken, P., Maute, A., Richmond, A. D., Vanhamaki, H., & Egbert, G. D. (2017). An application of principal component analyses to the interpretation of ionospheric currents. *Journal of Geophysical Research: Space Physics*, *122*, 5687–5708. https://doi.org/10.1002/2017JA024051

Bhattacharyya, A., & Okpala, K. C. (2015). Principal components of quiet time temporal variability of equatorial and low-latitude geomagnetic fields. *Journal of Geophysical Research: Space Physics*, *120*, 8799–8809. https://doi.org/10.1002/2015ja021673

Boudouridis, A., & Zesta, E. (2007). Comparison of Fourier and wavelet techniques in the determination of geomagnetic field line resonances. *Journal of Geophysical Research*, *112*, A08205. https://doi.org/10.1029/2006JA011922

Campbell, W. H. (1981). Annual and semiannual variations of the geomagnetic field at equatorial locations. *Journal of Atmospheric and Terrestrial Physics*, *43*(5–6), 607–616. https://doi.org/10.1016/0021-9169(81)90123-9

Campbell, W. H., & Matsushita, S. (1982). Sq currents: A comparison of quiet and active year behavior. *Journal of Geophysical Research*, *87*(A7), 5305–5308. https://doi.org/10.1029/ja087ia07p05305

Chen, G.-X., Xu, W.-Y., Du, A.-M., Wu, Y.-Y., Chen, B., & Liu, X.-C. (2007). Statistical characteristics of the day-to-day variability in the geomagnetic Sq field. *Journal of Geophysical Research*, *112*. https://doi.org/10.1029/2006ja012059

Chen, S. S., Denardini, C. M., Resende, L. C. A., Chagas, R. A. J., Moro, J., da Silva, R. P., et al. (2021). Evaluation of the Solar Quiet Reference Field (SQRF) model for space weather applications in the south America Magnetic Anomaly. *Earth Planets and Space*, *73*, 61. https://doi.org/10.1186/s40623-021-01382-8

Chen, S. S., Denardini, C. M., Resende, L. C. A., Chagas, R. A. J., Moro, J., & Picanço, G. A. S. (2020). Development of an empirical model for estimating the Quiet Day Curve (QDC) over the Brazilian sector. *Radio Science*, *55*. https://doi.org/10.1029/2020RS007105

Chulliat, A., Blanter, E., Le Mouël, J.-L., & Shnirman, M. (2005). On the seasonal asymmetry of the diurnal and semidiurnal geomagnetic variations. *Journal of Geophysical Research*, *110*, A05301. https://doi.org/10.1029/2004JA010551

Chulliat, A., Vigneron, P., & Hulot, G. (2016). First results from the Swarm dedicated ionospheric field inversion chain. *Earth Planets and Space*, *68*(104). https://doi.org/10.1186/s40623-016-0481-6

Cnossen, I., & Richmond, A. D. (2013). Changes in the Earth's magnetic field over the past century: Effects on the ionosphere–thermosphere system and solar quiet (Sq) magnetic variation. *Journal of Geophysical Research: Space Physics*, *118*, 849–858. https://doi.org/10.1029/2012JA018447

Cousins, E. D. P., Matsuo, T., Richmond, A. D., & Anderson, B. J. (2015). Dominant modes of variability in large-scale Birkeland currents. *Journal of Geophysical Research: Space Physics*, *120*, 6722–6735. https://doi.org/10.1002/2014ja020462

de Haro Barbas, B. F., Elias, A. G., Cnossen, I., & Zossi de Artigas, M. (2013). Long-term changes in solar quiet (Sq) geomagnetic variations related to Earth's magnetic field secular variation. *Journal of Geophysical Research: Space Physics*, *118*, 3712–3718. https://doi.org/10.1002/jgra.50352

Denardini, C. M., Chen, S. S., Resende, L. C. A., Moro, J., Bilibio, A. V., Fagundes, P. R., et al. (2018). The embrace magnetometer network for South America: Network description and its qualification. *Radio Science*, *53*, 288–302. https://doi.org/10.1002/2017RS006477

Fukushima, N. (1994). Some topics and historical episodes in geomagnetism and aeronomy. *Journal of Geophysical Research*, *99*(A10), 19113. https://doi.org/10.1029/94ja00102

Kerridge, D. J. (2001). *INTERMAGNET: Worldwide near-real-time geomagnetic observatory data*. Noordwijk, Netherlands. European Space Agency Space Weather Workshop, European Space Research and Technology Centre. Retrieved from www.intermagnet.org/publications/IM_ESTEC.pdf

Kirchhoff, V. W. J. H., & Carpenter, L. A. (1976). The day-to-day variability in ionospheric electric fields and currents. *Journal of Geophysical Research*, *81*(16), 2737–2742. https://doi.org/10.1029/ja081i016p02737

Laštovička, J. (2006). Forcing of the ionosphere by waves from below. *Journal of Atmospheric and Solar-Terrestrial Physics*, *68*(3–5), 479–497. https://doi.org/10.1016/j.jastp.2005.01.018

Le Sager, P., & Huang, T. S. (2002). Ionospheric currents and field-aligned currents generated by dynamo action in an asymmetric Earth magnetic field. *Journal of Geophysical Research*, *107*(A2), SIA–1. https://doi.org/10.1029/2001JA000211

Liu, L., Wan, W., Ning, B., Pirog, O. M., & Kurkin, V. I. (2006). Solar activity variations of the ionospheric peak electron density. *Journal of Geophysical Research*, *111*, A08304. https://doi.org/10.1029/2006JA011598

Mann, I. R., Milling, D. K., Rae, I. J., Ozeke, L. G., Kale, A., Kale, Z. C., et al. (2008). The upgraded CARISMA magnetometer array in the THEMIS Era. *Space Science Reviews*, *141*, 413–451. https://doi.org/10.1007/s11214-008-9457-6

Matsushita, S., & Maeda, H. (1965). On the geomagnetic solar quiet daily variation field during the IGY. *Journal of Geophysical Research*, *70*(11), 2535–2558. https://doi.org/10.1029/jz070i011p02535

Maute, A. (2017). Thermosphere-Ionosphere-Electrodynamics General Circulation Model for the Ionospheric Connection Explorer: TIEGCM-ICON. *Space Science Reviews*, *212*, 523–551. https://doi.org/10.1007/s11214-017-0330-3

Owolabi, C., Ruan, H., Yamazaki, Y., Li, J., Zhong, J., Eyelade, A. V., et al. (2021). Empirical Modeling of Ionospheric Current using Empirical Orthogonal Function Analysis and Artificial Neural Network. *Space Weather*, *19*(11). https://doi.org/10.1029/2021SW002831

Park, J., Lühr, H., & Min, K. (2011). Climatology of the inter-hemispheric field-aligned current system in the equatorial ionosphere as observed by CHAMP. *Annales Geophysicae*, *29*(3), 573–582. https://doi.org/10.5194/angeo-29-573-2011

Park, J., Yamazaki, Y., & Lühr, H. (2020). Latitude dependence of Interhemispheric Field-Aligned Currents (IHFACs) as observed by the Swarm constellation. *Journal of Geophysical Research: Space Physics*, *125*, e2019JA027694. https://doi.org/10.1029/2019JA027694

Pedatella, N. M., Forbes, J. M., & Richmond, A. D. (2011). Seasonal and longitudinal variations of the solar quiet (Sq) current system during solar minimum determined by CHAMP satellite magnetic field observations. *Journal of Geophysical Research*, *116*. https://doi.org/10.1029/2010ja016289

Pfaff, R., Larsen, M., Abe, T., Habu, H., Clemmons, J., Freudenreich, H., et al. (2020). Daytime dynamo electrodynamics with spiral currents driven by strong winds revealed by vapor trails and sounding rocket probes. *Geophysical Research Letters*, *47*. https://doi.org/10.1029/2020gl088803

Richards, P. G., Fennelly, J. A., & Torr, D. G. (1994). EUVAC: A solar EUV flux model for aeronomic calculations. *Journal of Geophysical Research*, *99*(A5), 8981–8992. https://doi.org/10.1029/94JA00518

Richmond, A. D. (1998). *The ionosphere and upper atmosphere. From the Sun: Auroras, Magnetic Storms, solar Flares, Cosmic Rays* (Vol. 50, pp. 35–44). Special Publications. https://doi.org/10.1029/sp050p0035

Richmond, A. D., & Roble, R. G. (1987). Electrodynamic effects of thermospheric winds from the NCAR thermospheric general circulation model. *Journal of Geophysical Research*, *92*(A11), 12365–12376. https://doi.org/10.1029/JA092iA11p12365

Schlapp, D. M., & Butcher, E. C. (1995). Seasonal and sunspot-cycle changes in the day-to-day variability of Sq. *Geophysical Journal International*, *120*(1), 173–185. https://doi.org/10.1111/j.1365-246x.1995.tb05919.x

Shore, R. M., Freeman, M. P., & Gjerloev, J. W. (2018). An empirical orthogonal function reanalysis of the northern polar external and induced magnetic field during solar cycle 23. *Journal of Geophysical Research: Space Physics*, *123*, 781–795. https://doi.org/10.1002/2017JA024420

Shore, R. M., Whaler, K. A., Macmillan, S., Beggan, C., Velímsky, J., & Olsen, N. (2016). Decadal period external magnetic field variations determined via eigenanalysis. *Journal of Geophysical Research: Space Physics*, *121*, 5172–5184. https://doi.org/10.1002/2015JA022066

Shume, E. B. B., Denardini, C. M. M., De Paula, E. R. R., & Trivedi, N. B. B. (2010). Variabilities of the equatorial electrojet in Brazil and Peru. *Journal of Geophysical Research*, *115*. https://doi.org/10.1029/2009JA014984

Soares, G., Yamazaki, Y., Cnossen, I., Matzka, J., Pinheiro, K. J., Morschhauser, A., et al. (2020). Evolution of the geomagnetic daily variation at Tatuoca, Brazil, from 1957 to 2019: A transition from Sq to EEJ. *Journal of Geophysical Research: Space Physics*, *125*, e2020JA028109. https://doi.org/10.1029/2020JA028109

Soares, G., Yamazaki, Y., Matzka, J., Pinheiro, K., Morschhauser, A., Stolle, C., & Alken, P. (2018). Equatorial counter electrojet longitudinal and seasonal variability in the American sector. *Journal of Geophysical Research: Space Physics*, *123*, 9906–9920. https://doi.org/10.1029/2018JA025968

Stening, R. J. (1971). Longitude and seasonal Variations of the Sq Current system. *Radio Science*, *6*(2), 133–137. https://doi.org/10.1029/rs006i002p00133

Stening, R. J. (1991). Variability of the equatorial electrojet: Its relations to the Sq current system and semidiurnal tides. *Geophysical Research Letters*, *18*, 1979–1982. https://doi.org/10.1029/91GL02413

Stening, R. J., & Winch, D. E. (2013). The ionospheric Sq current system obtained by spherical harmonic analysis. *Journal of Geophysical Research: Space Physics*, *118*, 1288–1297. https://doi.org/10.1002/jgra.50194

Takeda, M. (1990). Geomagnetic field variation and the equivalent current system generated by an ionospheric dynamo at the solstice. *Journal of Atmospheric and Terrestrial Physics*, *52*(1), 59–67. https://doi.org/10.1016/0021-9169(90)90115-4

Takeda, M. (1999). Time variation of global geomagnetic Sq field in 1964 and 1980. *Journal of Atmospheric and Solar-Terrestrial Physics*, *61*(10), 765–774. https://doi.org/10.1016/s1364-6826(99)00028-0

Takeda, M. (2002). Features of the global geomagnetic Sq field from 1980 to 1990. *Journal of Geophysical Research*, *107*(A9), 1252. https://doi.org/10.1029/2001JA009210

Takeda, M., & Yamada, Y. (1989). Quasi two-day period variation of the geomagnetic field. *Journal of Geomagnetism and Geoelectricity*, *41*(5), 469–478. https://doi.org/10.5636/jgg.41.469

Takeda, M., Yamada, Y., & Araki, T. (1986). Simulation of ionospheric currents and geomagnetic field variations of Sq for different solar activity. *Journal of Atmospheric and Terrestrial Physics*, *48*, 277–287. https://doi.org/10.1016/0021-9169(86)90103-0

Torta, J. M., Gaya-Piqué, L. R., Curto, J. J., & Altadill, D. (2009). An inspection of the long-term behavior of the range of the daily geomagnetic field variation from comprehensive modelling. *Journal of Atmospheric and Solar-Terrestrial Physics*, *71*(13), 1497–1510. https://doi.org/10.1016/j.jastp.2008.06.006

Vanhamäki, H., Maute, A., Alken, P., & Liu, H. (2020). Dipolar elementary current systems for ionospheric current reconstruction at low and middle latitudes. *Earth Planets and Space*, *72*, 146. https://doi.org/10.1186/s40623-020-01284-1

Weimer, D. R. (2005). Improved ionospheric electrodynamic models and application to calculating Joule heating rates. *Journal of Geophysical Research*, *110*. https://doi.org/10.1029/2004JA010884

Weimer, D. R. (2013). An empirical model of ground-level geomagnetic perturbations. *Space Weather*, *11*(3), 107–120. https://doi.org/10.1002/swe.20030

Xu, W.-Y., & Kamide, Y. (2004). Decomposition of daily geomagnetic variations by using method of natural orthogonal component. *Journal of Geophysical Research*, *109*, A05218. https://doi.org/10.1029/2003JA010216

Yamada, Y. (2009). Horizontal structure of the geomagnetic 2-day variation. *Journal of Geophysical Research*, *114*, A12312. https://doi.org/10.1029/2009JA014307

Yamashita, S., & Iyemori, T. (2002). Seasonal and local time dependences of the interhemispheric field-aligned currents deduced from the Ørsted satellite and the ground geomagnetic observations. *Journal of Geophysical Research*, *107*(A11), SIA–11. https://doi.org/10.1029/2002JA009414

Yamazaki, Y., Harding, B. J., Stolle, C., & Matzka, J. (2021). Neutral wind profiles during periods of eastward and westward equatorial electrojet. *Geophysical Research Letters*, *48*, e2021GL093567. https://doi.org/10.1029/2021GL093567

Yamazaki, Y., Häusler, K., & Wild, J. A. (2016). Day-to-day variability of midlatitude ionospheric currents due to magnetospheric and lower atmospheric forcing. *Journal of Geophysical Research: Space Physics*, *121*, 7067–7086. https://doi.org/10.1002/2016ja022817

Yamazaki, Y., & Maute, A. (2017). Sq and EEJ-A Review on the Daily Variation of the Geomagnetic Field Caused by Ionospheric Dynamo Currents. *Space Science Reviews*, *206*(1-4), 299–405. https://doi.org/10.1007/s11214-016-0282-z

Yamazaki, Y., Yumoto, K., Cardinal, M. G., Fraser, B. J., Hattori, P., Kakinami, Y., et al. (2011). An empirical model of the quiet daily geomagnetic field variation. *Journal of Geophysical Research*, *116*, A10312. https://doi.org/10.1029/2011JA016487

Yamazaki, Y., Yumoto, K., Uozumi, T., Abe, S., Cardinal, M. G., McNamara, D., et al. (2010). Reexamination of the Sq-EEJ relationship based on extended magnetometer networks in the East Asian region. *Journal of Geophysical Research*, *115*. https://doi.org/10.1029/2010ja015339

Yamazaki, Y., Yumoto, K., Uozumi, T., Yoshikawa, A., & Cardinal, M. G. (2009). Equivalent current systems for the annual and semiannual Sq variations observed along the 210°MM CPMN stations. *Journal of Geophysical Research*, *114*, A12320. https://doi.org/10.1029/2009JA014638

Yizengaw, E., & Moldwin, M. B. (2009). African Meridian B-field Education and Research (AMBER) Array. *Earth Moon Planet*, *104*(1), 237–246. https://doi.org/10.1007/s11038-008-9287-2

Yumoto, K., & the MAGDAS Group. (2006). MAGDAS project and its application for space weather, Solar Influence on the Heliosphere and Earth's Environment. In N. Gopalswamy, & A. Bhattacharyya (Eds.), *Recent Progress and Prospects* (pp. 309–405). http://magdas2.serc.kyushu-u.ac.jp/datausage/MAGDAS_ILWS_06.pdf